PHYSICAL REVIEW B **77**, 214521 (2008)

# Nonlinear Meissner effect in a high-temperature superconductor: Local versus nonlocal electrodynamics

D. E. Oates,[1] D. Agassi,[2] E. Wong,[3] A. Leese de Escobar,[3] and K. Irgmaier[4]
[1]*MIT Lincoln Laboratory, Lexington, Massachusetts 02420-9108, USA*
[2]*Naval Surface Warfare Center, Carderock Division, Bethesda, Maryland 20817, USA*
[3]*SPAWAR Systems Center, San Diego, California 92152-5001, USA*
[4]*THEVA Dünnschichttechnik GmbH, 85737 Ismaning, Germany*
(Received 4 March 2008; published 23 June 2008)

Measured intermodulation distortion (IMD) power at 1.5 GHz in a series of $YBa_2Y_3O_{7-\delta}$ stripline resonators of varying strip widths is compared to the predictions of two qualitatively distinct theories of the nonlinear Meissner effect. The stripline resonators are patterned from a single wafer to ensure uniformity of the material properties. According to the first theory [T. Dahm and D. J. Scalapino, Phys. Rev. B **60**, 13125 (1999)], the IMD power is dominated by contributions from the strip edges, while according to the second theory [D. Agassi and D. E. Oates, Phys. Rev. B **72**, 014538 (2005)] it is dominated by contributions from the body of the strip. The parameter-free comparison of the measured data with the theoretical predictions clearly favors the latter theory. We conclude that the nonlinear component of the penetration depth must be treated with nonlocal electrodynamics. The origins of this outcome are discussed briefly in the framework of a Green's-function approach.

DOI: 10.1103/PhysRevB.77.214521 PACS number(s): 74.78.−w, 74.70.−b, 85.25.−j

## I. INTRODUCTION

The nonlinear Meissner effect (NLME), as manifested for example in a current (or magnetic field) dependence of the penetration depth, was first predicted for the cuprate high-temperature superconductors (HTS) by Yip and Sauls[1] and extended to the intermodulation distortion (IMD) power and harmonic generation by Dahm and Scalapino (DS).[2] An alternative theoretical approach to the NLME was developed by Agassi and Oates (AO),[3] based on a perturbative expansion of the constitutive relation between the current and the vector potential. The NLME has been experimentally confirmed by IMD power measurements in high-quality $YBa_2Y_3O_{7-\delta}$ (YBCO) films, specifically, by observation of the characteristic low-temperature divergence of the IMD power $P_{\mathrm{IMD}}(T\rightarrow 0\ \mathrm{K})\sim T^{-2}$.[4–7] This low-temperature IMD power divergence agrees with the predictions of both DS and AO theories. Notwithstanding this agreement, the DS and AO theories are qualitatively distinct. In particular, the DS theory implies local electrodynamics for the NLME and, consequently, for thin films [$w \gg d$, Fig. 1(a)], $P_{\mathrm{IMD}}$ is dominated by contributions from the current crowding at the strip edges. On the other hand, the AO theory implies a nonlocal electrodynamics for the NLME, and consequently $P_{\mathrm{IMD}}$ is dominated by contributions from the strip midsection (see below). The work reported here tests experimentally which of these two qualitatively distinct theories applies.

One way to formulate the distinction between the DS and the AO theories for the NLME is to focus on the corresponding low-power penetration-depth expansions,

$$\lambda = \lambda_0 + \lambda_{\mathrm{NL}} = \left\{ \begin{array}{ll} \lambda_0 + \lambda_2(\mathrm{AO})(I/d)^2 + \ldots & (\mathrm{AO}) \\ \lambda_0 + \lambda_2(\mathrm{DS}) j_S^2(y,z) + \ldots & (\mathrm{DS}) \end{array} \right\}, \tag{1.1}$$

where $\lambda_0$ and $\lambda_{\mathrm{NL}}$ denote the linear (London) and the nonlinear terms in the penetration-depth expansion. $\lambda_2(\mathrm{AO})$ and $\lambda_2(\mathrm{DS})$ are coefficients (of different dimensionality) that do not depend on the strip dimensions, $d$ denotes the strip thickness in the notation of Fig. 1(a), and $I$ denotes the total microwave current in the strip,

$$I = \int j_S(y,z)\,dy\,dz. \tag{1.2}$$

In Eq. (1.2) $j_S(y,z)$ is the pair-current density, thereby implicitly assuming that the broken-pair current is negligible in comparison. For the AO theory, the expansion in Eq. (1.1) has been derived in Ref. 3. For the DS-theory, the expansion Eq. (1.1) follows from the standard penetration-depth expression $\lambda^2 = mc^2/(4\pi q_S^2 n_S)$,[8] where $m$ and $q_S$ denote the single-carrier mass and charge (positive or negative), respectively, and $n_S$ denotes the Cooper-pair single-carrier density. We use the cgs unit system throughout this paper. Inserting in the above penetration-depth expression the decomposition $\lambda = \lambda_0 + \lambda_{\mathrm{NL}}$, $\lambda_{\mathrm{NL}} \ll \lambda_0$ and the corresponding Cooper-pair density expansion, $n_S(y) = n_S^{(0)} + n_S^{(2)} j_S^2(y,z) + \ldots$,[2] yields the DS-theory expansion in Eq. (1.1). According to Eq. (1.1), a possible experimental comparison of the DS and AO theories would be to measure the dependence of the IMD power on the strip thickness $d$, i.e., $P_{\mathrm{IMD}}(d)$. In the AO theory $P_{\mathrm{IMD}}(d) \propto d^{-4}$,[9] while in the DS theory the thickness dependence is considerably weaker. Such an experiment, however, is impractical due to the considerable difficulties of growing high-quality, thick YBCO films that maintain good epitaxy. Consequently, we focus on the measurement of $P_{\mathrm{IMD}}(w)$, the dependence of the IMD power on the strip width [Fig. 1(a)]. This observable is experimentally accessible, e.g., by measuring $P_{\mathrm{IMD}}(w)$ in a series of stripline resonators of varying widths all of which are patterned from the same wafer to ensure uniformity. The predictions of the AO and DS theories for $P_{\mathrm{IMD}}(w)$ are significantly different (see below), and

 

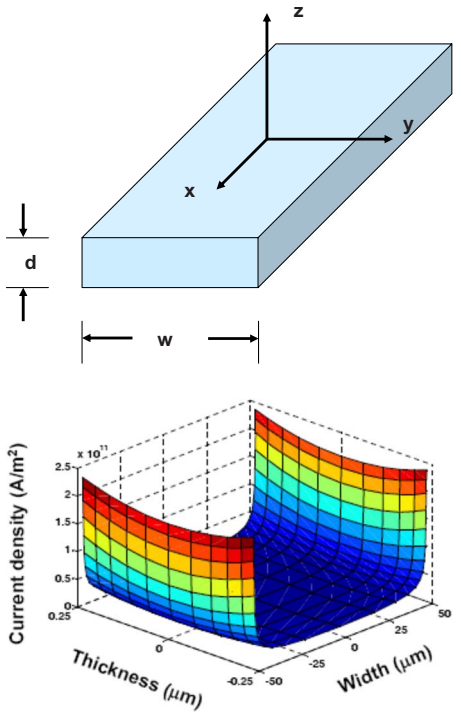


FIG. 1. (Color online) (a) The choice of coordinate system and definition of the width $w$ and thickness $d$ parameter in a generic thin film strip $w \gg d$. (b) An example of a numerically exact calculation of the pair-current density $j_S(y,z)$ for a typical strip, where $w=100$ $\mu$m, $d=500$ nm, and $\lambda_0=250$ nm. The circulating current is 0.026 mA. Note the negligible thickness dependence, which consequently is neglected throughout this work. Note also that the calculation is made with a linear (current-independent) penetration depth, and for the circulating currents considered in these experiments, we assume that the current distribution is independent of the circulating current because the changes in $\lambda$ are much less than 0.1% (Ref. 5). Thus, the current density shown scales linearly with the total circulating current.

the parameter-free comparison of the data with the predictions, Eq. (2.7) below, is based on the distinct *structures* of the corresponding penetration-depth expansions in Eq. (1.1).

Expansions (1.1) expose a qualitative distinction between the DS and AO theories. In the latter, the nonlinear penetration depth is spatially constant and depends on $\langle j_S(y,z)\rangle_{y,z}=I/(wd)$, or equivalently, on the *total* current $I$.[3] Since in a thin-film the preponderance of the total current is carried in its midsection, it follows that the midsection contributions for $\lambda_{\mathrm{NL}}$ are dominant. On the other hand, in the DS theory $\lambda_{\mathrm{NL}}$ tracks the spatial dependence of the *local* current density $j_S(y,z)$. Consequently, since $j_S(y,z)$ is strongly peaked at the edges of the stripline,[10] those edge contributions are dominant for $\lambda_{NL}$. As shown in the next section, this qualitative difference between the DS and AO transcribes into significantly different predictions.

The paper is organized as follows: In Sec. II we derive the expressions for $P_{\mathrm{IMD}}(T,I;w)$ of the DS and AO theories in the low-power regime. Sec. III provides experimental details and the methodology of extracting the data. Sec. IV is devoted to the comparison of the data with the theoretical predictions. In Sec. V we discuss the comparison between the DS and AO theories and the corresponding small parameter that controls the convergence of the expansions Eq. (1.1). The last section is a summary. The two Appendices describe some of the mathematical details.

## II. THEORETICAL BACKGROUND

We start by briefly reviewing the relationship between the measured $P_{\mathrm{IMD}}$ and the penetration-depth expansions, Eq. (1.1). This relationship is established in two steps. First, $P_{\mathrm{IMD}}$ is connected to the strip inductance, which has a nonlinear term, i.e., a term that depends on current, while the second step connects the nonlinear inductance to the nonlinear term of the penetration depth $\lambda_{\mathrm{NL}}$ in Eq. (1.1). Explicitly, the first step states that

$$P_{\mathrm{IMD}} \propto (IL_{\mathrm{NL}})^2, \tag{2.1}$$

where all constants irrelevant to the considerations below have been suppressed[3] and the nonlinear inductance term $L_{\mathrm{NL}}$ of the total inductance $L$ is defined by

$$L = L_0 + L_{\mathrm{NL}}, \quad L_{\mathrm{NL}} \ll L_0, \tag{2.2}$$

with self-explanatory notation. Note that implicit in Eqs. (2.1) and (2.2) $L$ is the modeling of the physical resonator with an equivalent circuit. Although the nonlinear resistance also contributes to the IMD power, we consider only the contribution of the nonlinear inductance as it has been shown to be the dominant component.[5]

To calculate $L_{\mathrm{NL}}$ we assume, as Dahm and Scalapino,[2] that $L_{\mathrm{NL}}$ is associated primarily with the kinetic inductance through the nonlinear term in the penetration-depth decomposition $\lambda_{\mathrm{NL}} \ll \lambda_0$, Eq. (1.1). To conform with the stripline resonator geometry in our experiments,[4,5] where $d=0.5$ $\mu$m, the current density is assumed uniform through the thickness dimension $z$ and the strip can be considered as of infinite length. Figure 1(b) is a plot of the calculated $j_S(y,z)$ for the stripline geometry used in our measurements for a 100-$\mu$m-wide line.[10] The thickness independence of $j_S(y,z)$ is evident. Thus, hereinafter we assume a one-dimensional current density $j_S=j_S(y)$. Furthermore, for a stripline long compared to the penetration depth it is suggestive to introduce the inductance per unit length $\Lambda$ such that $L=2\ell\Lambda/\pi^2$ and $\ell$ denotes the strip's length.[4,5] Combining Eq. (2.1) with these considerations yields for the nonlinear inductance term the expression,

$$L_{\mathrm{NL}} = \frac{2\ell}{\pi^2}\Lambda_{\mathrm{NL}}, \quad \Lambda_{\mathrm{NL}} \propto \frac{\lambda_0}{I^2}\int dA\lambda_{\mathrm{NL}} j_S^2(y), \tag{2.3}$$

where $\Lambda_{\mathrm{NL}}$ is the nonlinear part of the inductance per unit length and $A$ denotes integration over the strip cross section. The proportionality factor in Eq. (2.3) is of no consequence in the following. Inserting expansions Eq. (1.1) into Eq. (2.3) yields the key relations,

$$L_{\mathrm{NL}} \propto \Lambda_{\mathrm{NL}} \propto \begin{cases} \int dA \lambda_2(\mathrm{AO})(I/d)^2 j_S^2(y) & (\mathrm{AO}) \\ \int dA \lambda_2(\mathrm{DS}) j_S^4(y) & (\mathrm{DS}) \end{cases}. \tag{2.4}$$

The DS-theory expression for $L_{\mathrm{NL}}$ in Eq. (2.4) has been derived before.[1]

Expressions Eq. (2.4) in conjunction with Eq. (2.1) underscore that according to the DS theory, $P_{\mathrm{IMD}}$ in *thin-film* strips is dominated by contributions from the edges due to the strongly peaked $j_S^4(y)$ factor in the integrand. On the other hand, the corresponding factor in the AO theory is $j_S^2(y)$; hence the edge contributions are of considerably less importance than those from the midsection of the strip. This qualitative observation suggests $P_{\mathrm{IMD}}(T,w)$, at a fixed temperature $T$, as a natural observable for which the DS and AO theories yield considerably different predictions. The following heuristic argument further substantiates this conjecture. In a thin film, the current densities at its edges, $j_S(w/2)$ and at its midpoint, $j_S(0)$, are approximately related by $j_S(w/2) = C j_S(0)\sqrt{w}$, where $C$ is a constant.[11] However, $j_S(0) \sim I/(wd)$. Therefore $I \propto j_S(w/2)\sqrt{w}$ or

$$j_s(w/2) \propto \frac{I}{\sqrt{w}}. \tag{2.5}$$

Equation (2.5) implies that for a fixed $I$, variation of the strip width $w$ generates a corresponding current-density variation at the strip edges. In conjunction with Eqs. (2.4) and (2.1) such a variation implies a width dependence $P_{\mathrm{IMD}}(T,w)$ that is more pronounced in the DS theory than in the AO theory. We measure and calculate this signature in this work.

The $P_{\mathrm{IMD}}$ data is conventionally expressed in dimensionless dBm units, defined by

$$P_{\mathrm{IMD}}(\mathrm{dBm}) = 10 \log_{10}\left(\frac{P_{\mathrm{IMD}}}{1mW}\right). \tag{2.6}$$

Accordingly, straightforward manipulations with Eqs. (2.1), (2.4), and (2.6) yield

$$P_{\mathrm{IMD}}(\mathrm{dBm};w) - P_{\mathrm{IMD}}(\mathrm{dBm};w_0) = \begin{cases} 20 \log_{10}\left(\dfrac{\int dA j_S^2(y;w)}{\int dA j_S^2(y;w_0)}\right) & (\mathrm{AO}) \\ 20 \log_{10}\left(\dfrac{\int dA j_S^4(y;w)}{\int dA j_S^4(y;w_0)}\right) & (\mathrm{DS}), \end{cases} \tag{2.7}$$

where $w_0$ denotes a reference width and the total current $I$ is kept fixed regardless of the $w$ variable.

The relation Eq. (2.7) is central to this work. Its left-hand side is measured while its right-hand side is a *parameter-free* calculable expression (see below). Note that Eq. (2.7) hinges on the *structure* of the expansions in Eq. (1.1) rather than the particular values of the pertinent coefficients. Furthermore, provided experiments are confined to the low-power and low-temperature domains, for which expansion Eq. (1.1) is valid, the right-hand side of Eq. (2.7) is independent of the total current $I$. While Eq. (2.7) is nominally independent of temperature, it is experimentally advantageous to measure at low temperatures in order to minimize effects of inadvertent vortex motion. For the calculations, the current density $j_s(y;w)$ in Eq. (2.7) must be numerically evaluated for the configuration at hand.[10] As shown below in Eq. (4.2), there is also a good, simple analytic approximation to the right-hand side of Eq. (2.7).

## III. EXPERIMENT

The measurements were carried out on stripline resonators fabricated from a single $YBa_2Y_3O_{7-\delta}$ film deposited on a 2-inch-diameter lanthanum aluminate $LaAlO_3$ (LAO) wafer. The films were deposited by a reactive-evaporation technique that has been described previously.[12] Reference 12 and references contained therein also present the properties of the films deposited by this method. The transition temperature is very close to 90 K and the doping level is close to optimum. LAO is the preferred substrate for this investigation since high-quality samples on LAO have been shown to exhibit intrinsic nonlinearities.[4,5] YBCO films deposited on other substrates, such as sapphire and MgO, do not exhibit intrinsic nonlinearity due to induced defects in the YBCO film for a sapphire substrate[9] and due to substrate nonlinearities in the case of an MgO substrate.[13]

The films were patterned using standard photolithography and wet etching. All resonators were patterned simultaneously in a single process step to assure uniformity. After patterning, the wafer was diced and the etched striplines were assembled with YBCO ground planes to form stripline resonators. The properties of the patterned line dominate the performance of the resonator because the current density is approximately a factor of 100 higher in the line than in the ground plane. We used linewidths of $w=25$, 50, 75, 100, 150, and 300 $\mu$m. The corresponding characteristic line impedances are $Z_0=42$, 40, 38, 36, 33, and 26 $\Omega$, respectively.

The resonators were measured by a technique that has been described previously,[4,5] in which the quality factor $Q$ and resonant frequency $f_0$ of the resonator are measured as a function of the microwave power at temperatures between 5 K and $T_c$. The measurements were carried out at the fundamental frequency of 1.5 GHz. The third-order IMD was measured in the usual way, in which two closely spaced tones of equal power at frequencies $f_1$ and $f_2$ are combined and applied to the resonator. The frequencies are centered about the resonant frequency with a tone separation of approximately 1/32 of the low-power 3-dB bandwidth. The frequencies of the tones were adjusted at each power level and temperature to maintain the same relationship to the bandwidth and resonant frequency. The power $P_{\mathrm{IMD}}$ of the third-order mixing products at frequencies $2f_1-f_2$ and $2f_2-f_1$ is then measured in a spectrum analyzer as a function of the input power to the resonator. For the analysis of the data, the measured $P_{\mathrm{IMD}}$ is

converted to a normalized IMD power $P_{\mathrm{NORM}}$, which removes the dependence of the IMD on resonator unloaded $Q$ value and insertion loss.[4]

$$P_{\mathrm{NORM}} = \frac{P_{\mathrm{IMD}}}{r_v(1-r_v)Q_c}. \tag{3.1}$$

In Eq. (3.1) $r_v$ denotes the voltage insertion ratio, which is related to the insertion loss IL in dB by

$$r_v = 10^{-\mathrm{IL}/20}, \tag{3.2}$$

and $Q_c$ is the unloaded $Q$ of the resonator. In addition, the input power $P$ is converted to microwave current associated with the standing wave in the resonator at resonance according to the expression

$$I = \sqrt{\frac{4Q_l r_v P}{\pi Z_0}}. \tag{3.3}$$

In Eq. (3.3) $Q_l$ denotes the loaded $Q$ value. The data are then plotted as normalized IMD power $P_{\mathrm{NORM}}$ vs microwave current $I$.

### A. Comparison of the calculated and measured $Q$

Before presenting the data, we compare the calculated $Q$ values of the resonator with the measured values. This comparison serves as a consistency check of the numerically calculated current distribution, since the calculated unloaded $Q$ value involves an integral of the current distribution squared as we show now. The $Q_c$ is given by

$$Q_c = \frac{\omega\Lambda}{R}, \tag{3.4}$$

where $\omega$ is the angular frequency and $R$ is its resistance per unit length. The impedance of the line is

$$Z = \sqrt{\frac{\Lambda}{C}}, \tag{3.5}$$

where $C$ is the capacitance per unit length. Since $\omega \sim 1/\sqrt{\Lambda C}$, Eqs. (3.4) and (3.5) yield

$$Q_c \sim \sqrt{\frac{1}{\Lambda C}}\frac{\Lambda}{R} \sim \sqrt{\frac{\Lambda}{C}}\frac{1}{R} \sim \frac{Z}{R}, \tag{3.6}$$

where $R$ is given by[10]

$$R = \frac{2R_S\lambda_0 \int j_S^2(y,z)dydz}{\left|\int j_S(y,z)dydz\right|^2}. \tag{3.7}$$

In Eq. (3.7) $R_S$ denotes the surface resistance, and $j_S(y,z)$ is the current distribution in the coordinate system of Fig. 1(a).

Figure 2 shows the measured and calculated [from Eq. (3.6)] $Q_c$ values at $T=5$ K at the fundamental frequency and low input power as a function of the linewidth for the resonators used in this study. By comparing the calculated and measured $Q_c$ of the 25-$\mu$m line, we determine the product

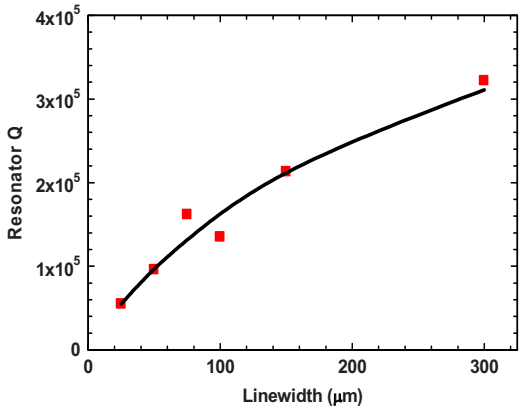


FIG. 2. (Color online) Calculated and measured resonator $Q$ as a function of linewidth. Points are measured and line is calculated. The uncertainty of the measurement is estimated to be 10%. The calculation was normalized to the $Q$ of the 25-$\mu$m line. This is equivalent to determining the $R_S$ and $\lambda$ of the film from the measurement of the 25-$\mu$m linewidth.

$R_S\lambda_0$ in Eq. (3.7). This product is then assumed to be identical for all of the resonators under investigation. The agreement between the calculated and measured $Q_c$ in Fig. 2 is very good. This is an independent validation of the current distribution employed in Eq. (2.7), which is used to calculate the $P_{\mathrm{IMD}}$ in Sec. IV. This agreement is also a verification that the actual active linewidth is given by the patterned, photolithographically determined linewidth, and that damage to the edges resulting from the etching is negligible. It has been previously shown by this group by comparing surface resistance measurements on the same film, first unpatterned and then patterned, that patterning of the stripline does not induce damages that alter the microwave properties.[14]

### B. Measurements of intermodulation distortion

Typical IMD power vs $I$ data in the low-power regime for the 75-$\mu$m-wide line is shown in Fig. 3 for several selected temperatures. More temperatures were measured and analyzed but are omitted from the figure for clarity. To confirm that the measured IMD has an intrinsic origin, the inset shows the characteristic IMD power divergence at low temperatures $P_{\mathrm{IMD}}(T\to 0\ \mathrm{K}; w=75\ \mu\mathrm{m}) \to T^{-2}$ (Refs. 3–5).

To compare the DS and AO theories, the data for the left-hand side of Eq. (2.7) is obtained as follows. To comply with the basic weak-power assumption where expansion (1.1) applies, we focus on the available, very low-current IMD data. The chosen low-current domain, however, should be sufficiently high for a good signal-to-noise ratio in the data. The points in the double logarithmic plot, Fig. 4, present the normalized IMD data vs $I$ at $T=5$ K for the series of the linewidth values quoted in the caption. Note that for a given current, the normalized IMD increases as the line becomes narrower. This trend reflects the increased current density as the line narrows for fixed total current. The low-current data points in Fig. 4 are fitted with straight lines of slope 60 dBm per decade of current by a standard least-squares procedure. The slope of 60 dBm per decade of cur-

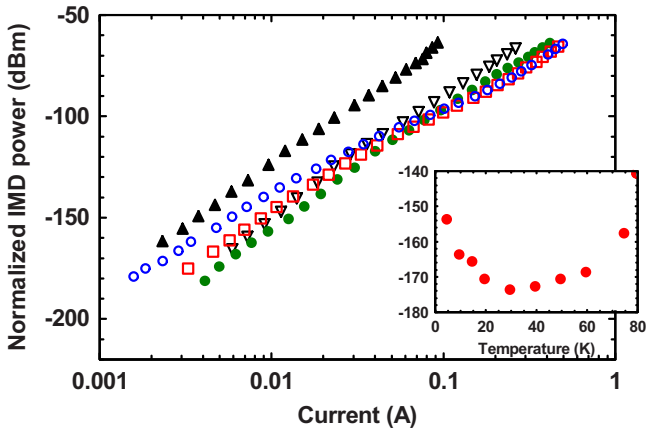


FIG. 3. (Color online) An example of $P_{\mathrm{IMD}}(\mathrm{dBm};I,T)$ data for a strip with $w=75$ $\mu$m plotted against the current $I$. The open circle, the open squares, the full circles, the open inverted triangles, and the full triangles correspond to the temperatures $T=5$, 10, 30, 60, and 80 K, respectively. The inset is a plot of $P_{\mathrm{IMD}}(\mathrm{dBm};I=0.005\ \mathrm{A},T)$ against the temperature to demonstrate the low $T$ divergence as a signature for intrinsic nonlinearity.

rent corresponds to slope 3 of the $P_{\mathrm{NORM}}$ vs circulating power on double logarithmic plots that has been discussed elsewhere,[3–5] and the chosen current domain $0.0015 \leq I \leq 0.003$ A is consistent with the low-circulating-power considerations above. From these fitted lines we extract the IMD power vs linewidth for the left-hand side of Eq. (2.7). This procedure has been repeated for each of the measured temperatures up to 60 K. To save space, we show only the data at $T=5$ K. The other temperatures produce comparable results.

## IV. RESULTS

### A. Comparison with theory

In Figs. 5 and 6 we compare the measured data with the theoretical predictions of Eq. (2.7). Figure 5 shows the result of averaging over the temperatures of 5, 10, 15, 20, 30, 40, 50, and 60 K, while Fig. 6 contains only data at $T=5$ and 10 K. The error bars on the data in Fig. 5 represent one standard deviation. The chosen reference width in Eq. (2.7) is $w_0=25$ $\mu$m. The *only* input parameters in the numerical calculations of the right-hand side of Eq. (2.7) [involving the numerically calculated current density $j_S(y,z)$ [11]] are the penetration depth $\lambda_0(T)$ and the stripline thickness. The results are not very sensitive to either of the parameters. Otherwise, as emphasized above, the right-hand side of Eq. (2.7), when applied in its range of validity, does not depend either on $I$ or $T$. The $I$ independence is automatically guaranteed by the linear fitting in Fig. 4, while the predicted $T$ independence is used as a consistency check for the data analysis and is vindicated by the relatively small error bars in Fig. 5 and temperature variation in Fig. 6. For the samples in our experiment, the corresponding values are $\lambda_0(T=0)=250$ nm and $d=500$ nm. As the data in Figs. 5 and 6 convincingly show, the difference between the local DS and the nonlocal AO theoretical predictions is considerably larger than the error

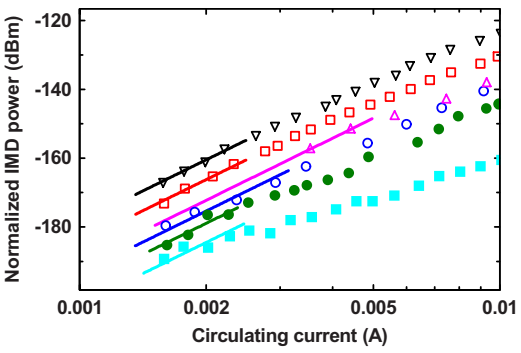


FIG. 4. (Color online) Data points for $P_{\mathrm{IMD}}(\mathrm{dBm};I,T=5\ \mathrm{K},w)$ at the low-power regime and the corresponding fitted lines according to the methodology described in Sec. III. The linewidths are ∇25 $\mu$m, □50 $\mu$m, Δ75 $\mu$m, ○ 100 $\mu$m, ● 150 $\mu$m, and ■ 300 $\mu$m.

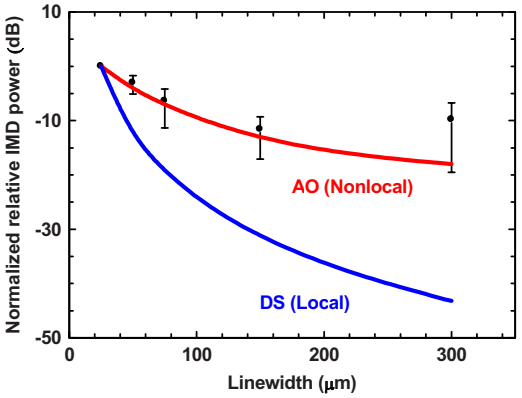


FIG. 5. (Color online) Comparison of the $P_{\mathrm{IMD}}(\mathrm{dBm};w)$ data with the theoretical predictions of the DS and AO theories, Eq. (2.7). The 25-$\mu$m line is used as the reference. The data error bars represent the spread of the data points with $T$ in the range $5 \leq T \leq 60$ K. The calculations (solid lines) are with the exact numerical current density, such as in Fig. 1(b) using the method in Ref. 10 (see text).

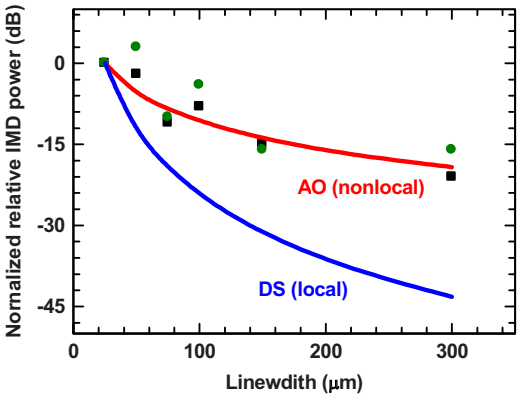


FIG. 6. (Color online) Comparison of the $P_{\mathrm{IMD}}(\mathrm{dBm};T,w)$ data at only 5 and 10 K with the theoretical predictions of the DS and AO theories [Eq. (2.7)]. The 25-$\mu$m line is used as the reference. The symbols ● and ■ correspond to the temperatures $T=5$ and 10 K, respectively.

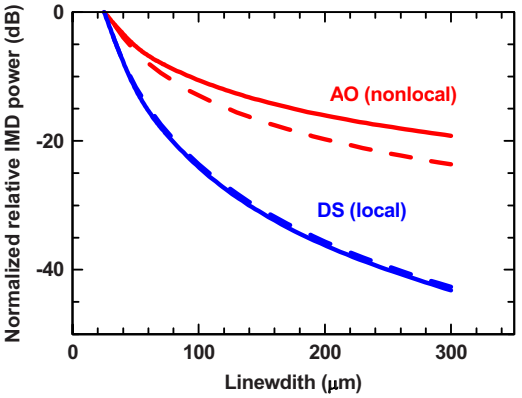


FIG. 7. (Color online) Comparison of the exact numerical calculation (solid line) and the analytical approximation derived from Eq. (4.2) (broken line). The 25-$\mu$m line is used as the reference. Note the close resemblance of the exact numerical calculations and the analytical approximation.

bars, and the nonlocal AO theory predictions track the data. Furthermore, as argued after Eq. (2.5), the IMD variation according to the AO theory is indeed smaller than those in the DS theory.

### B. Analytic approximation

Beside the $Q_c$-values comparison in Fig. 2, a second check on the numerical calculations of the right-hand side of Eq. (2.7) is an analytical approximation, displayed by the broken line in Fig. 7. This approximation is based on an expression of the current density $j_S(y)$ for a long, thin strip ($w \gg d$).[11] Specifically, in the coordinate system of Fig. 1(a) consider the approximate current density,

$$j_S(y) = \begin{cases} \dfrac{j_S(0)}{\sqrt{1-\left(\dfrac{2y}{w}\right)^2}} & \text{for} \quad |y| \le \left(\dfrac{w}{2}\right)\left(1-\dfrac{t}{w}\right) \\ 0 & \text{for} \quad \dfrac{w}{2} \ge |y| \ge \left(\dfrac{w}{2}\right)\left(1-\dfrac{t}{w}\right) \end{cases}, \tag{4.1}$$

where $t \approx \lambda_0^2/d$ and the strip cross section extends to $y = \pm w/2$. Note the explicit strip-width dependence in Eq. (4.1) and that the sole penetration-depth dependence enters through the cutoff parameter $t$. Since typically for our thin films $t/w \sim 10^{-3} \ll 1$, it seems justified to neglect the portion in Eq. (4.1) that diverges beyond the cutoff point. Although the contribution of this omitted portion of current density to $P_{\mathrm{IMD}}$ is substantial in the DS theory, we verified numerically that it is still far too small in comparison to the differences between the AO and DS theories predictions for $P_{\mathrm{IMD}}$. Inserting Eq. (4.1) into Eq. (2.7) and employing the closed-form integrals and approximation detailed in Appendix yields the approximate expressions,

$$P_{\mathrm{IMD}}(\mathrm{dBm};w) - P_{\mathrm{IMD}}(\mathrm{dBm};w_0) = \frac{20}{\ln(10)} \times \begin{cases} \ln\left[\dfrac{w \ln\left(\dfrac{2w}{t}\right)}{w_0 \ln\left(\dfrac{2w_0}{t}\right)}\right] & (\mathrm{AO}) \\ \ln\left[\dfrac{w^2 + tw \ln\left(\dfrac{2w}{t}\right)}{w_0^2 + tw_0 \ln\left(\dfrac{2w_0}{t}\right)}\right] & (\mathrm{DS}). \end{cases} \tag{4.2}$$

As Fig. 7 shows, the expression in Eq. (4.2) provides a very good approximation to full numerical calculations of the right-hand side of Eq. (2.7). This provides another validation of the nontrivial exact numerical calculations.

The $P_{\mathrm{IMD}}(w)$ data in Figs. 5 and 6 agree with the nonlocal AO theory. This agreement adds to previous experimentally confirmed predictions of the AO theory regarding the temperature dependence of the $P_{\mathrm{IMD}}(T)$ data, including the low-temperature divergence of $P_{\mathrm{IMD}}(T \to 0\ \mathrm{K}) \sim T^{-2}$,[3–5] the nonmonotonic slope of $P_{\mathrm{IMD}}(P_{\mathrm{CIRC}})$,[15] and indications that $P_{\mathrm{IMD}}(d) \sim d^{-4}$, as in Eq. (1.1).[9] Since these IMD data sets represent distinct cuts of the $P_{\mathrm{IMD}}(T,I,..;w,d,..)$ function in its multiple parameter space, the ability to account for them all in the low-power domain lends credence to validity of the nonlocal AO theory for intrinsic nonlinearity.

A practical implication of the experimental verification of the AO theory is that film edges are less important for $P_{\mathrm{IMD}}$ than previously believed. For microwave receive-filter design, this result indicates that damage to the strip edges during the stripline patterning is not a major degrading factor in their performance.

## V. DISCUSSION

The experimental results for $P_{\mathrm{IMD}}(w)$ presented here clearly favor the AO theory over the alternative DS theory. On the other hand, both theories yield the same prediction for the low-temperature divergence $P_{\mathrm{IMD}}(T \to 0\ \mathrm{K}) \sim T^{-2}$, which has been experimentally confirmed. As highlighted in the basic penetration-depth expansions, Eq. (1.1), a key distinction between the DS and AO theories is that the former is local while the latter is nonlocal.[3,14] In this section, we discuss briefly the origin of these results.

Underlying the DS theory is the two-fluid model where the total current density $\vec{j}$ is the sum of pair-current density $\vec{j}_S = n_S q_S \vec{v}_S$ and the quasiparticle current density $\vec{j}_{\mathrm{QP}}$ ('backflow'). The NLME originates from the $\vec{j}_{\mathrm{QP}}$ component. The latter is expressed in terms of $f_{\mathrm{QP}}$, the quasiparticle distribution function,

$$f_{\mathrm{QP}}(\vec{j}_S;T) = \frac{1}{e^{\beta e}+1}, \quad e = E + (\vec{v}_S \bullet \vec{k}). \tag{5.1}$$

where $E = \sqrt{\xi^2 + \Delta^2}$, $\beta = 1/\sqrt{k_B T}$, $T$ is the temperature, $k_B$ is the Boltzmann constant, $\vec{k}$ is the momentum, $\Delta$ is the energy gap,

$\xi=\varepsilon(\vec{k})-\mu$ is the single-particle excitation energy $\varepsilon(\vec{k})$ with respect to the chemical potential $\mu$, $v_S$ is the superfluid velocity, related to $\vec{j}_S$ and the pair density and charge $n_S$, $q_S$, respectively.

Bardeen[16] derived the distribution function (5.1) in the context of a quasiparticle Fermi-gas model in the presence of a *spatially uniform*, weak current density. The local feature of the DS theory [e.g., Eq. (1.1)] emanates from applying the distribution function Eq. (5.1) to the thin-film case of a *spatially nonuniform* current density $\vec{j}_S(x)$. By employing the Green's-function approach of Ref. 3, it can be shown that for a spatially nonuniform current density the quasiparticle distribution function in Eq. (5.1) must be complemented by terms that involve higher derivatives of $\vec{j}_S(x)$ and thus indicates nonlocality.

In conjunction with the NLME, the nonlocality property is important according to the following plausibility argument. Since that condensate motion (current) breaks pairs, it is plausible to expect that the amount of local pair-breaking and the amount of local current correlate. In thin films, where $w \gg d \sim \lambda$, the overwhelming majority of current is carried in its broad midsection. This is verified from the Eq. (A3) by varying $t$ such that $w/2 \geq t \geq 0$. Accordingly, it follows that the majority of quasiparticles are generated in the film midsection. These quasiparticles are accounted for in the AO nonlocal theory by taking the long-wavelength limit. On the other hand, the local DS theory overemphasizes the strip edges. Hence it accounts only for a fraction of the quasiparticles and therefore it does not track the data quantitatively. This argument may clarify why both the DS and the AO theories yield the same prediction for the low-temperature divergence $P_{\mathrm{IMD}}(T \to 0\ \mathrm{K}) \sim T^{-2}$. As pointed out elsewhere this divergence reflects the low-energy quasiparticle excitations along the nodal lines of the $d$-wave gap of YBCO.[1] These are present throughout the strip, regardless of their spatial distribution, and therefore both theories predict the same temperature divergence. Also, note that the $P_{\mathrm{IMD}}(w)$ observable probes the current-density distribution across the entire film, and hence it exposes the qualitative difference between the DS and AO theories.

In summary, measurements of the width dependence of the IMD power in a stripline resonator at a constant total current are analyzed and compared to predictions of two theories of the nonlinear Meissner effect. The measured strips were patterned from a single wafer to ensure uniformity of film quality. This data is compared to predictions of the local theory of Dahm and Scalapino,[2] where the nonlinear penetration depth tracks the local current density, and of the theory of Agassi and Oates,[3] where the nonlinear penetration depth is spatially constant. The parameter-free comparison between the data and theoretical predictions at several temperatures clearly favors the AO predictions. We attribute this outcome to a key qualitative distinction between the AO and DS theories, i.e., the locality vs nonlocality as articulated, e.g., in Eq. (1.1).

## ACKNOWLEDGMENTS

The work at NSWC-Carderock Division was supported by the ILIR program of NSWC Carderock. The work at Lincoln Laboratory was supported in part by AFOSR and in part by SPAWAR System Center. The work at SPAWAR System Center was supported by the SPAWAR System Center ILIR program.

## APPENDIX

For the approximate current-density expression Eq. (4.1), the integrals underlying Eq. (2.7) in closed form are

$$\int_0^{(w/2)(1-t/w)} dy j_S^2(y;w) = -\frac{w}{2}\arctan h\left(\frac{t-w}{w}\right),$$

$$\int_0^{(w/2)(1-t/w)} dy j_S^4(y;w) = -\frac{w}{4t(t-2\mathrm{w})}\left[w(-t+w)+t(2w+t)\arctan h\left(1-\frac{t}{w}\right)\right]. \tag{A1}$$

The actual expressions given in Eq. (4.2) are based on approximating Eq. (A1) by

$$\arctan h(1-x) = \frac{1}{2}\ln\left(\frac{2-x}{x}\right) \approx \frac{1}{2}\ln\left(\frac{2}{x}\right), \quad \text{for} \quad x \ll 1. \tag{A2}$$

For the total current considerations, the following integral is useful to note,

$$\int_0^{(w/2)(1-t/w)} dy j_S(y;w) = -\frac{w}{2}\arcsin\left(\frac{t-w}{w}\right). \tag{A3}$$

[1] S. K. Yip and J. A. Sauls, Phys. Rev. Lett. **69**, 2264 (1992); D. Xu, S. K. Yip, and J. A. Sauls, Phys. Rev. B **51**, 16233 (1995); B. P. Stojkovic and O. T. Valls, *ibid.* **51**, 6049 (1995).

[2] T. Dahm, D. J. Scalapino, and B. A. Willemsen, J. Supercond. **12**, 339 (1999); T. Dahm and D. J. Scalapino, Phys. Rev. B **60**, 13125 (1999); T. Dahm and D. J. Scalapino, Appl. Phys. Lett. **81**, 2002 (1997).

[3] D. Agassi and D. E. Oates, Phys. Rev. B **72**, 014538 (2005).

[4] D. E. Oates, S.-H. Park, and G. Koren, Phys. Rev. Lett. **93**, 197001 (2004); D. E. Oates, S. H. Park, D. Agassi, and G. Koren, Supercond. Sci. Technol. **17**, S290 (2004).

[5] D. E. Oates, J. Supercond. Novel Magn. **20**, 3 (2007).

[6] K. T. Leong, J. C. Booth, and S. A. Schima, IEEE Trans. Appl. Supercond. **15**, 3608 (2005).

[7] G. Cifariello, M. Aurino, E. Di Gennaro, G. Lamura, P. Orgiani, J.-C. Villégier, X. X. Xi, and A. Andreone, J. Phys.: Conf. Ser. **43**, 702 (2006).

[8] M. Tinkham, *Introduction to Superconductivity*, 2nd ed.

(McGraw-Hill, New York, 1996).
[9] D. E. Oates, S.-H. Park, D. Agassi, G. Koren, and K. Irgmaier, IEEE Trans. Appl. Supercond. **15**, 3589 (2005).
[10] D. M. Sheen, S. M. Ali, D. E. Oates, R. S. Withers, and J. A. Kong, IEEE Trans. Appl. Supercond. **1**, 108 (1991).
[11] T. Van Duzer and C. W. Turner, *Principles of Superconductive Devices and Circuits* (Elsevier, NewYork, 1981).
[12] R. Semerad, J. Kauf, K. Irgmaier and W. Pruseit, Physica C, **378-381**, 1414 (2002).
[13] M. A. Hein, D. E. Oates, P. J. Hirst, R. G. Humphreys, and A. V. Velichko, Appl. Phys. Lett. **80**, 1007 (2002).
[14] Hao Xin, D. E. Oates, A. C. Anderson, R. L. Slattery, G. Dresselhaus, and M. S. Dresselhaus, IEEE Trans. Microwave Theory Tech. **48**, 1221 (2000).
[15] D. Agassi and D. E. Oates, Phys. Rev. B **74**, 024517 (2006).
[16] J. Bardeen, Phys. Rev. Lett. **1**, 399 (1958).